ORNL/TM-2021/2300

Subcriticality Measurements for a Changing Concentration Uranyl Nitrate Solution Tank by Californium Source-Driven Noise Analysis

John T. Mihalczo

December 2021

OAK RIDGE National Laboratory

ORNL IS MANAGED BY UT-BATTELLE LLC FOR THE US DEPARTMENT OF ENERGY

ORNL/TM-2021/2300

Physics Division

SUBCRITICALITY MEASUREMENTS FOR A CHANGING CONCENTRATION URANYL NITRATE SOLUTION TANK BY CALIFORNIUM SOURCE-DRIVEN NOISE ANALYSIS

John T. Mihalczo

December 2021

Prepared by
OAK RIDGE NATIONAL LABORATORY
Oak Ridge, TN 37831-6283
managed by
UT-BATTELLE, LLC
for the
US DEPARTMENT OF ENERGY
under contract DE-AC05-00OR22725

CONTENTS

LIST OF FIGURES

LIST OF TABLES

ABSTRACT

Subcritical californium source-driven noise analysis measurements were performed at the Oak Ridge Critical Experiments Facility in 1983 using a stainless-steel tank with an inside diameter of 76.2 cm and a height of 90 cm but only filled with a uranyl (93.16 wt. % ^{235}U) nitrate solution to a height of 76.2 cm for all measurements. The free acid content of the uranyl nitrate solution was less than 0.01 N to minimize hazards in handling. The total available uranium for these measurements was 5,296 g. The concentration of the solution was varied from the highest density of 14.71 grams of uranium per liter (g U/L) initially in 16 steps, lowering the concentration to 0.3492 g U/L, and finally using a tank filled with only water. The tank had a Plexiglas lid to minimize evaporation. The Cf source was contained in a re-entrant Plexiglas tube which could be in the solution parallel to the axis of the cylindrical tank. The detectors were ^{3}He proportional counters in the solution in shrink-fit tubing to isolate the counters from the fissile solution and adjacent to the outside of the tank. In some cases, the detectors were scintillators adjacent to the outside of the tank. In other cases, the source was external to the tank. Some data presented in this report are from notes and are not in the logbook. The purpose of this report is to document the experimental information for the measurements performed so that later, researchers could perform the required uncertainty and calculational analyses and documentation to use these data for an International Nuclear Criticality Safety Benchmark Program (ICSBEP) or a Nuclear Energy Agency benchmark. The data from these measurements are available from the Records Management Services Department of Oak Ridge National Laboratory, and the logbook is available from John Bess of ICSBEP at Idaho National Laboratory.

This work is part of a cooperative program (funded by Idaho National Laboratory [INL]) between INL and Oak Ridge National Laboratory (ORNL) to extensively document the details of a wide variety undocumented critical and subcritical experiments (>15) performed by ORNL at ORCEF and other USDOE critical experiment facilities that utilized hundreds (>500) of operational days of critical facility time (described in ORNL/TM-2019/18).

1. INTRODUCTION

These measurements supported by the Y-12 Plant Nuclear Criticality Safety group were performed between May 9 and July 19, 1983, and used 66 operational days at the Oak Ridge Critical Experiments Facility (ORCEF). The californium source-driven noise analysis (CSDNA) method was used [1] to determine the neutron multiplication factor for a uranyl nitrate solution tank with varying uranium concentration [2]. The stainless-steel tank with an inside diameter of 76.2 cm and a height of 91.4 cm was only filled with a uranyl (93.16 wt. % ^{235}U) nitrate solution to a height of 76.2 cm for all measurements. The free acid content of the uranyl nitrate solution was less than 0.01 normal to minimize hazards in handling. The total available uranium for these measurements was 5,296 g. The concentration of the solution was varied in 16 steps, from the highest density of 14.71 grams of uranium per liter (g U/L) initially, lowering the concentration to 0.3492 g U/L, and finally using a tank filled with only water. The source and detector location was varied and included locations inside and outside the tank. The ^{3}He proportional counters were placed in the solution with their axes parallel to the axis of the cylindrical tank, and the scintillators were adjacent to the outer radial surface of the tank.

The purpose of this report is to document the configuration of fissile material and the online data that were acquired during the measurements so that at some later time researchers could use these data to benchmark nuclear criticality safety calculations for the International Criticality Safety Benchmark Program (ICSBEP) and the European Atomic Energy Agency's Nuclear Energy Agency (NEA) benchmarks. Some of the data presented were not from logbooks but from auxiliary notes. Some of these

data are from notes and the author's memory and not in the logbooks. Co-experimenters in these measurements are Elizabeth B Johnson, Willie T. King and Edward D. Blakeman. The experimental logbook for this experiment is Oak Ridge National Laboratory (ORNL) logbook H00228-Solution Tanks-1983 [3] available from ORNL's Records Management Services Department and the ICSBEP at Idaho National Laboratory (INL)

This work is part of a cooperative program (funded by Idaho National Laboratory [INL]) between INL and Oak ORNL to extensively document the details of a wide variety undocumented critical and subcritical experiments (>15) performed by ORNL at ORCEF and other USDOE critical experiment facilities that utilized hundreds (>500) of operational days of critical facility time (described in ORNL/TM-2019/18 [4]).

2. DESCRIPTION OF THE CONFIGURATION

In this section, the experimental tank, the uranyl nitrate solution at the various dilutions, the Cf source, and the detectors are described.

2.1 DESCRIPTION OF THE TANK

The cylindrical stainless-steel (304) tank had an inside diameter of 76.2 cm, a height of 91.4 cm, and a wall thickness of 0.32 cm. The bottom of the tank was 1.27 cm thick, and the tank had a 1.27-cm-thick, 76.2-cm.-squate Plexiglas lid to minimize evaporation. The lid was reinforced for stiffness with two 6-in.-high gussets the width of the lid and each 12 in. from the center. The Plexiglas lid had four radial 1-in.-wide slots (90° apart) and two slots 30° from those at 90° (Oak Ridge National Laboratory [ORNL] drawing QSK-GWA-830406 [5]). These slots provided access for location of the source and detectors in the solution. The tank had a 0.32-cm-thick, 5.08-cm-high rim tack welded at the top for rigidity. The tank was mounted on a carbon steel angle support with the bottom of the tank 76.2 cm above a grated carbon steel floor (2.51 cm thick) of the West cell of the ORCEF. Above the grated floor was a thin (~0.050 cm thick) stainless steel sheet to prevent leakage through the grate to the ground floor of the West cell. A 1-in. schedule 40 stainless-steel pipe about 15 in. long and flanged to accept a valve was welded through the bottom near the circumference to facilitate draining the solution. This grating was 3.6 m above the concrete floor of the experiment cell. The cell in which the tank was located was ~9.1 × 12.2 × 9.1 m high, with thick concrete walls and roof. The experiment vessel was located 4.7 m from the 9.1-m south side of the cell, 3 m from the 12.2-m east side, and ~1.85 m from a 2.9-m-diameter empty steel tank (2.5 cm thick walled) that was also present in the cell. The empty steel tank was located 6.2 m from the 12.2-m east side of the cell.

Before adding the fissile solution, the tank was calibrated by adding water in 20-L batches and observing the height of the water in the tank. The increments were then reduced to between 340 and 350L, the latter being the desired height of the fissile solution. The calibration indicated that 350 L corresponded to a solution height of 77 cm and that negligible variations existed in the inside diameter with height. It was decided to fill the tank with a solution height of 76.2 cm which was also the inside diameter of the tank.

2.2 DESCRIPTION OF THE SOLUTION

The uranyl nitrate solution, in which the uranium was enriched to 93.16 wt. % ^{235}U, was received at the ORCEF in five nominally 10-L bottles at a concentration of about 106 g U/L. The total inventory available for the measurements was 5,296 g of uranium. This solution was then diluted with demineralized water to a concentration of 14.71 g U/L, which was the initial concentration for the experiments. The diluted solution was transferred by means of a peristaltic (fingers) pump from the 10-L

bottles to into the 76.2 cm inside diameter tank. The transfer of the solution was monitored in the presence of a neutron source with external neutron detectors that supplied signals to the counting channels (with audible signals proportional to the count rate), and a steady-state count rate was measured after each bottle of diluted solution was transferred. These neutron multiplication measurements were used to confirm that the system when filled was subcritical and near the desired neutron multiplication. After the measurement with the initial solution concentration, the solution was diluted in 16 steps with CSDNA measurements at each step. After each dilution, the removed sample solution was returned to the Y-12 Plant for chemical analysis. After the final dilution, the tank was drained, rinsed, and filled with demineralized water for the final measurements.

The isotopic composition is the average of two measurements and is given in Table 1 where it has been retyped from the data page 298 of the logbook.

Table 1. Isotopic composition.

Uranium isotope	Weight percent[a]
^{234}U	1.010
^{235}U	93.16
^{236}U	0.440
^{238}U	5.490

[a]Average of two measurements

The impurities determined by spectrochemical analysis are given in Table 2 which has been retyped from the data on page 268 of the logbook. Except for those listed in the table, the other impurities were lower than the detectable limit. The analysis was performed for two samples. The free acid content is low to minimize hazards in handling.

Table 2. Impurity content of the uranyl nitrate solution.

After first dilution	Element	Content
	Mg	2 ppm
	Al	2 ppm
	Cu	35 ppm
	Na	3 ppm
	C	60 ppm
	Free acid	<0.01 N
After second dilution	Be	0.1 ppm
	Mg	5 ppm
	Al	5 ppm
	Ca	10 ppm
	Fe	20 ppm
	Na	15 ppm
	Si	20 ppm
	C	60 ppm
	Free acid	< 0.01 N

The results of the chemical analysis are given in Table 3 for the 16 different dilutions of the solution. The highest uranium content of uranyl nitrate was added to the solution tank first and then diluted by adding demineralized water and removing excess solution. After each addition, the removed solution was sent from ORCEF to the Y-12 Plant for analysis. The compositions of uranyl nitrate, $UO_2 (NO_3)_2$, are given in Table 3 which has been retyped from the chemical analysis from Logbook page number 278.

Table 3. Summary of chemical analysis of the uranium nitrate.

Dilution number	g U/g of solution	Solution density (g/cm^3)	g U/L	(g ^{235}U/L	Molar ratio (U/N)	Total nitrate (µg NO_3 per g)	pH	Logbook page Number
1	0.01445[a]	1.0177[a]	14.71	13.70	0.505	7,591	2.62	24
2	0.013610	1.0170	13.84	12.89				91
3	0.013070	1.0158	13.28	12.37				105
4	0.012690	1.0160	13.89	12.01				123
5	0.011720	1.0140	11.88	11.07				162
6	0.010600	1.0123	10.73	9.996				175
7	0.009524	1.0108	9.627	8.968				187
8	0.008419[b]	1.0093	8.497	7.916	0.501	4,419	2.76	193
9	0.006941[b]	1.0073	6.992	6.513	0.497	3,663	2.81	200
10	0.005750[b]	1.0055	5.781	5.386	0.502	3,036	2.87	213
11	0.004756	1.0040	4.775	4.448				221
12	0.003653	1.0030	3.664	3.413				230
13	0.002714	1.0010	2.717	2.531				238
14	0.001350	0.9995	1.356	1.263				245
15	0.000679	0.9985	0.6780	0.632				252
16	0.000349	0.9981	0.3493	0.325				256
Water	0.000000	1.000	0.000	0.000	--			259

[a]Average of six determinations
[b]Average of two determinations

2.3 DESCRIPTION OF THE CALIFORNIUM SOURCE

The ^{252}Cf was electroplated on one plate of a parallel-plate ionization chamber, and the spontaneous fission rate was ~55,000/s (~0.1 µg ^{252}Cf). Two Cf sources (ORNL identification CF 19 and ORNL identification Cf 20) were fabricated at the same time with approximately the same fission rates; a sketch is given in Figure 1. The source was located both inside the solution and adjacent to the outside of the cylindrical tank with the Cf deposit in close proximity to the tank wall. Californium source Cf 19 was used inside the tank in the solution in a liquid-tight Lexan tube. The source ionization chamber was mounted at the end of 1.90-cm- outside diameter, 1.27-cm- inside diameter Lexan tubes with the signal cable from the chamber inside the Lexan tube (Figure 2). The sources were sealed from the solution with shrink tubing and epoxy. The Lexan tubing and the signal cable protruded out the top of the solution through the lid of the experimental vessel. The lid had a slot so the Lexan tube could be located at various radial positions. The Lexan tube was parallel to the axis of the cylinder. The source could be located vertically anywhere along the axis of the cylindrical experimental vessel. Californium source 20 was used only adjacent to the outside radial surface of the cylindrical tank with the californium deposit adjacent to the tank wall. Thus, the axis of Cf 20 outside the tank was along a radius and that of Cf 19 inside the tank was parallel to the cylindrical tank axis.

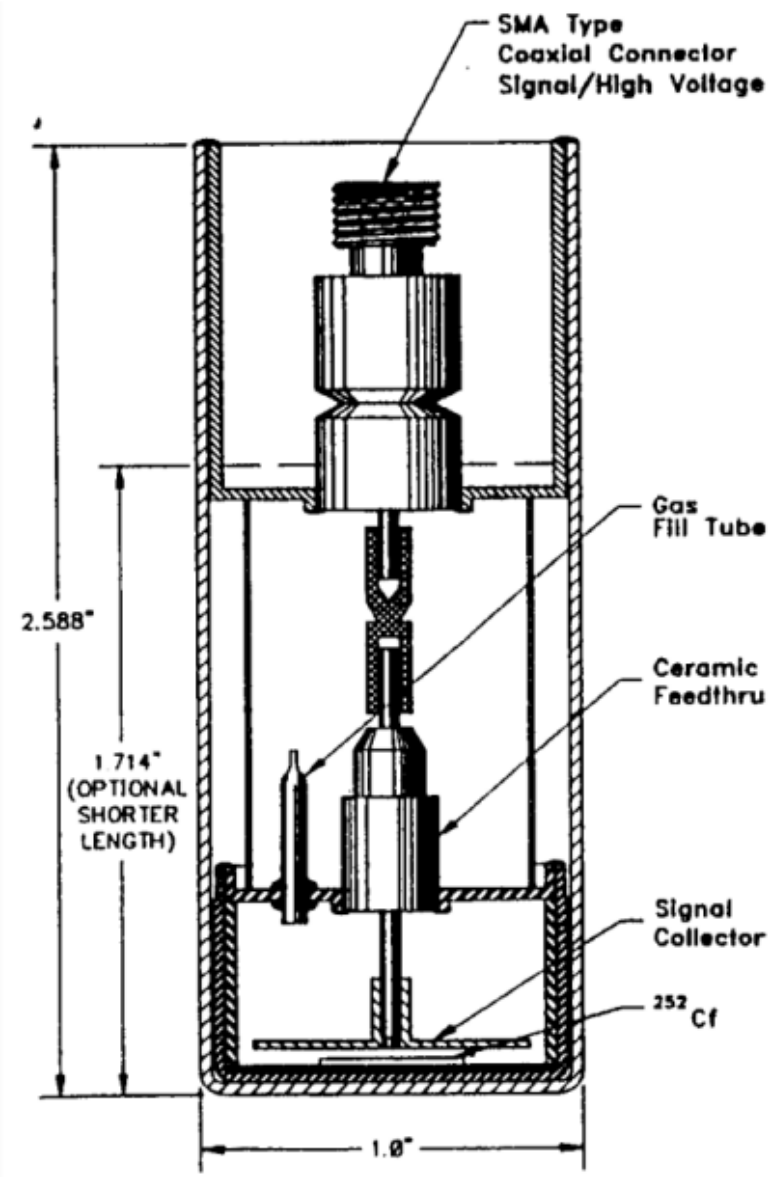

Figure 1. Configuration of the Cf ionization chamber (Cf not to scale).

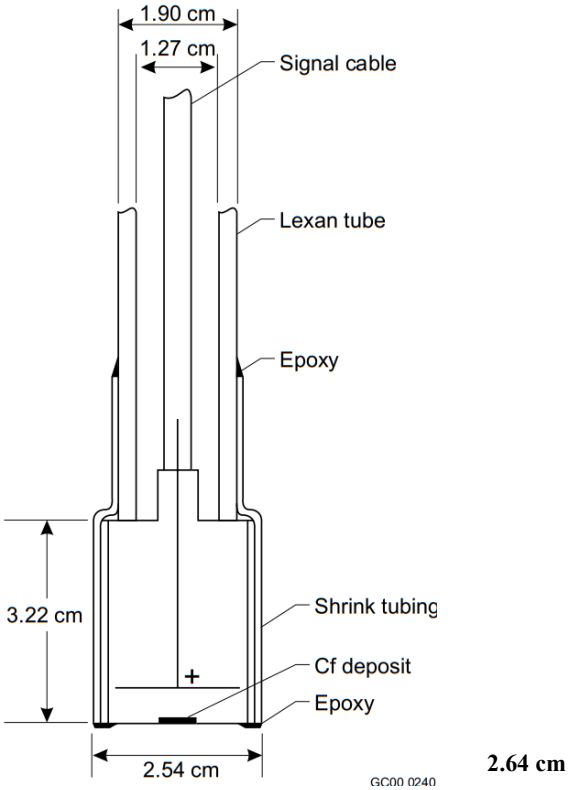

Figure 2. Configuration of the Cf sources at the end of the Lexan tube.

A detailed Monte Carlo N-Particle (MCNP) model of the Cf ionization chamber is given in Appendix A from previous ICSBEP/NEA benchmarks, SUB-HEU-SOL-THERM-001 and -002 [6, 7]. Either of these two documents has the MCNP input files for the source and would be useful for preparing an MCNP input file for calculations.

2.4 DESCRIPTION OF DETECTORS

The CSDNA method requires two detectors. The detector types used in these measurements were unshielded enriched Li glass scintillation detectors external to the tank and ^{3}He proportional counters in the solution that could be located at different radii. The detectors in the solution were in thin-walled, tight-fitting, plastic shrink-fit tubing to isolate them from the fissile solution. The researchers used Reuter Stokes model number RSN-42A (1-in. outside diameter, 12-in.-length) ^{3}He proportional counters, which were located symmetrically about the vertical midplane of the solution with their axes parallel to the cylindrical tank axis.

The scintillation detectors were composite Li-glass scintillation detectors that had sensitivity to neutrons and gamma rays caused by proton-recoil interactions in the organic material to slow neutrons caused by interactions with the ^{6}Li glass. The neutron and gamma sensitive detector (ORNL Drawing Q-5167-1 [8]) consisted of a photomultiplier tube (RCA C7151Q) optically coupled to a 3.81-cm, 2.54-cm-thick Li (6.6 wt. % Li, enriched to 95%) glass scintillator (Nuclear Enterprises, NE-905). A sketch of the scintillation detectors is given in Figure 3. Identical detectors were used in these experiments and on opposite side of the cylindrical assembly. These detectors were also located adjacent to the outside of the tank about 180° apart.

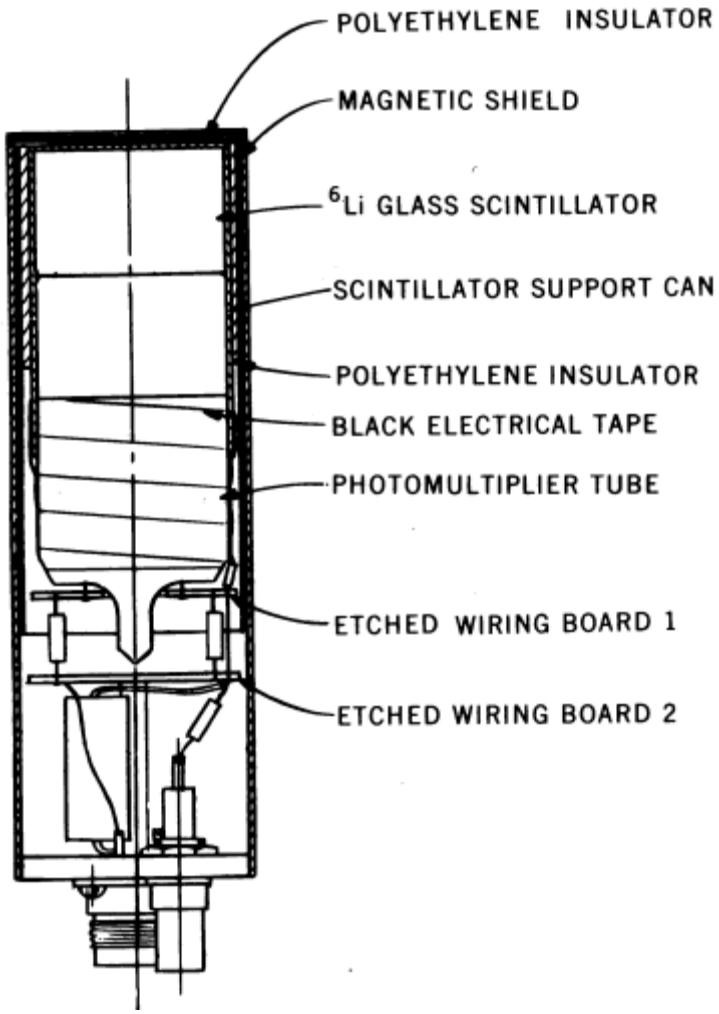

Figure 3. Sketch of the scintillation detector (inside the support can was a plastic light pipe).

3. MEASUREMENT RESULTS

The measurement configuration including the source and detector locations are listed in Appendix B. The detector signals were transmitted over ~100-foot-long cables outside the ORCEF to a trailer where the data processing and analysis systems were located.

3.1 RATIO OF SPECTRAL DENSITIES FOR THE CSDNA MEASUREMENT

The CSDNA subcriticality determination measures a ratio of spectral densities which is obtained from the auto and cross power spectral densities of the source and two detection channels. The CSDNA experiments measure the Fourier transforms of the time domain cross correlation functions between each of the two detectors and the source emission. These correlation functions are the equivalent of a randomly pulsed neutron measurement in the time domain. These two Fourier transforms are designated as G_{S1} and G_{S2}. The cross correlation function of the two detectors is measured and is the equivalent of a two-detector Rossi alpha measurement. This two-detector correlation function is also Fourier transformed to give G_{12}. The time distribution of counts in the source ionization chamber with respect to a previous count in the source ionization chamber is also Fourier transformed to give the auto power spectral density of the source, G_{SS}. These cross and auto correlation functions transforms are combined in a ratio of spectral

densities, G_{S1}* G_{S2}/ Gss G_{23}, where * means complex conjugation. This ratio is independent of detection efficiency because the same detection efficiencies appear in the numerator and denominator and their cancellations result in the independence. This ratio was originally formulated for use in approach to criticality measurements to avoid the problems associated with detection efficiency and source effectiveness with the modified source neutron multiplication method, which was usually the way to monitor the approach to critical. The ratio is constant at low frequencies and averages over the frequency range where it is constant and is used to obtain the neutron multiplication factor using a point kinetics model to infer the neutron multiplication factor, k_{eff}. The CSDNA on-line results for the measurement of the ratio of spectral densities at low frequency are given in Appendix C. Appendix C also provides the values of the coherence between detectors. The coherence between two detectors $(\gamma_{12})^2$ is (G^*_{12} times G_{12})/ (G_{11} times G_{22}). For final analysis, these data should be reexamined to confirm the online results given here.

Two different point kinetics models exist for interpretation of the ratios of spectral densities—a Pare/Mihalczo formulation [1] and an Akcasu/Stolle formulation [9]. At low neutron multiplication factors (<0.80) the latter formulation gives the neutron multiplication factor much higher than actual. Some of these differences from previous measurements are described in Appendix D.

The ratios of spectral densities were interpreted using calculated values of the parameters required to infer the k_{eff} from the ratio. These values are given for the central source location in Table 4 along with the break frequency, f_b, which is related to the prompt neutron decay constant, α, by the relationship $\alpha = 2\pi f_b$. The break frequency is defined in Appendix E, and an example of the fitting of data from another measurement is provided. The table also includes calculated neutron multiplication factors. Two formulations of point kinetics were used to obtain the neutron multiplication factor. Appendix F gives the parameters used to obtain the neutron multiplication factor from the ratio of spectral.

Table 4. Neutron multiplication factors from KENO calculations and from the ratios of spectral densities and break frequencies as a function of measured solution concentration with the source in the center of the solution.

^{235}U (g/L)	Calculated neutron multiplication factor	Ratio of spectral densities	K_{eff} from measurements Pare/Mihalczo	K_{eff} from measurements (Akcasu/Stolle)	Break frequency (s^{-1})
13.70	0.91402	0.170	0.932	0.934	166.92
12.89	0.86867	0.225	0.903	0.908	204.67
12.37	0.89457	0.255	0.885	0.893	258.32
12.01	0.85379	0.280	0.869	0.879	245.75
11.07	0.82097	0.315	0.849	0.848	289.55
9.996	0.77126	0.370	0.800	0.823	339.43
8.986	0.72392	0.410	0.762	0.792	387.31
7.935	0.67762	0.46	0.710	0.753	435.84
6.505	0.59811	0.535	0.613	0.685	501.04
5.362	0.52033	0.610	0.490	0.608	455.79
4.448	0.45515	0.635	0.450	0.585	599.01
3.413	0.36916	0.680	0.3195	0.504	62341
2.531	0.28977	0.735	0.154?	0.434?	688.15
1.263	0.15658	0.83	–	–	747.28
0.632	0.08215	0.835	-	–	776.67
0.325	0.04311	0.860	-	-	791.09

The ratios of spectral densities are plotted in Figure 4 for the central source location are plotted as a function of solution concentration. As expected, the ratio of spectral densities equals 0.9 with no uranium in the solution (plain water in the tank), as predicted by the Pare/Mihalczo formulation. The k_{eff} values from the ratio of spectral densities with the two different point kinetics formulations of the theory are compared with calculations as a function of solution concentration in Figure 5.

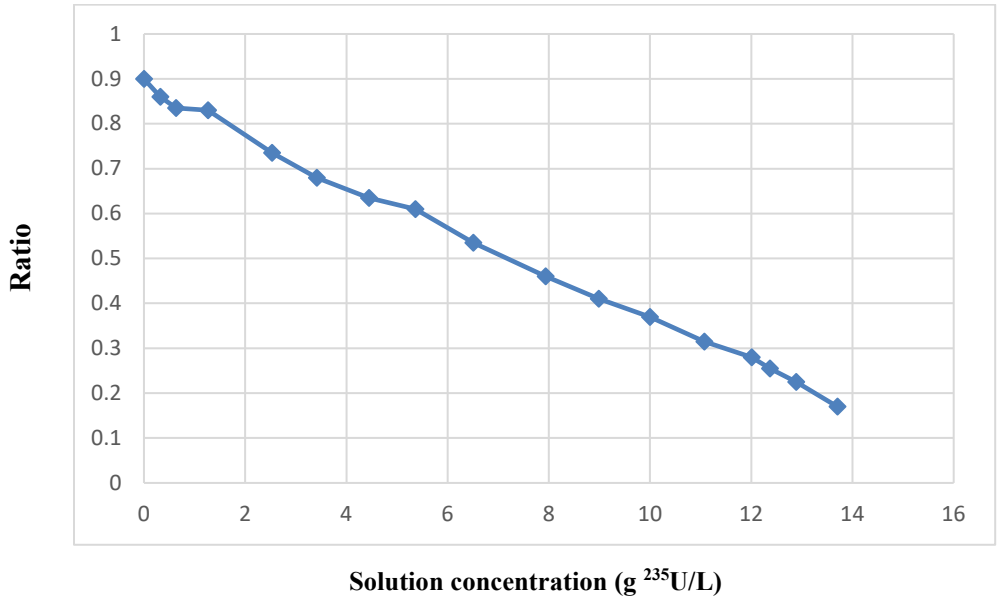

Figure 4. Measured ratio of spectral densities as a function of solution concentration for the central source location.

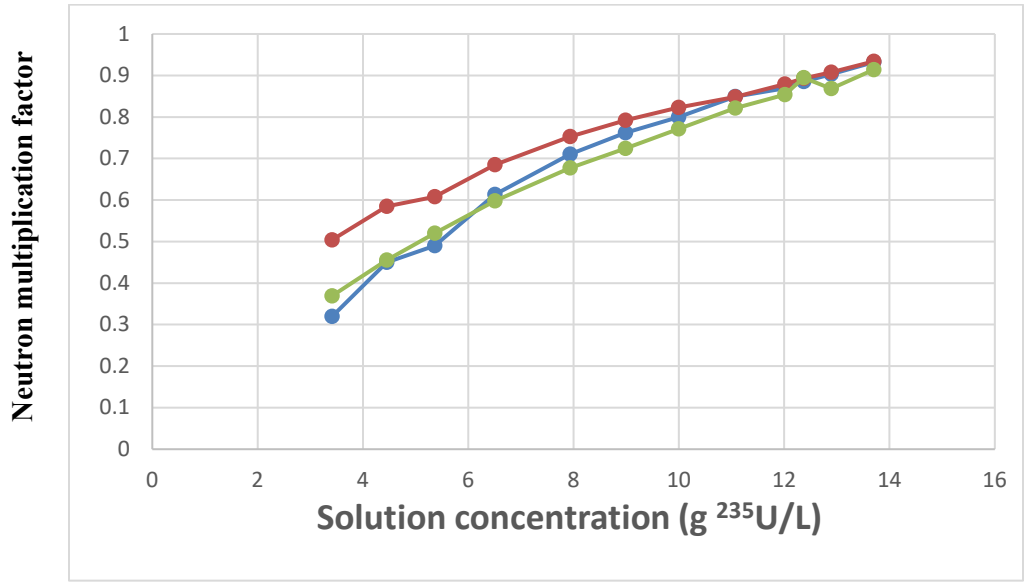

Figure 5. Comparison of neutron multiplication factor, k_{eff} from measurements with calculation as a function of solution concentration.(Blue—Mihalczo/Pare formulation, red—Akcasu/Stolle formulation, gray—KENO calculations).

The data of Figure 4 extrapolate to 0.89 at zero solution concentration, which is consistent with other previous measurements [10] in air with a time-tagged Cf source and two large plastic scintillation

detectors (sensitive to fast neutron above 1 MeV) at different distances from the source. In these measurements with the large plastic scintillators, only the neutron part of the time-of-flight distribution was used to form the auto and cross power spectral densities used for the ratio of spectral densities. Effectively, this was gamma discrimination by time of flight. These time-of-flight measurements gave a ratio of spectral densities for the neutron only of 0.89. The measurements reported here at zero solution concentration and the previous measurements in air and with large water bottles agree with the value of the ratio of spectral densities from the Pare/Mihalczo formulation for the ratio of spectral densities. This formulation predicts a value equal to the average square of the number of neutrons from Cf fission divided by the square of the average number of neutrons from Cf fission $\langle \nu^2 \rangle / (\langle \nu \rangle)^2$ where < > means average. This value is 0.893 for Cf fission using the data from Reference 10.

The k_{eff} values with the Akcasu/Stolle formulation are consistently higher than those from the Pare/Mihalczo formulation with significant differences at k_{eff} values less than 0.80. These differences have been observed in all other measurements, one of which is described in Appendix D.

3.2 PROMPT NEUTRON DECAY CONSTANT FROM BREAK FREQUENCY NOISE ANALYSIS

The frequency dependence of the auto and cross power spectral densities [9] can be fitted to obtain the prompt neutron decay constant. The break frequency and an example of the fitting process is given in Appendix E from another measurement. The prompt neutron decay constants obtained as a function of solution concentration are given in Figure 6.

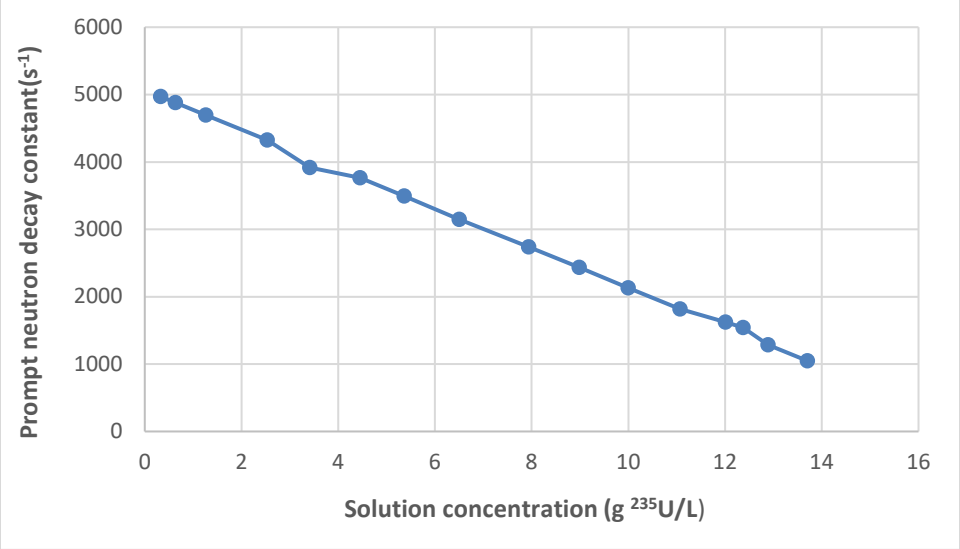

Figure 6. Prompt neutron decay constant vs solution concentration.

Several methods can be used to calculate the prompt neuron decay constant. Thus, the measured prompt neutron decay constant can also be used to benchmark calculational methods.

4. CONCLUSIONS

These californium source driven noise analysis (CSDNA) measurements for a uranyl nitrate solution tank with varying (16 steps including only water and no uranium) uranium (93.16 wt.% ^{235}U) concentration are accurately described and are suitable for benchmarking calculations. The ratios of spectral densities were interpreted by two different point kinetics formulation: the Pare/Mihalczo formulation, in which the first

detection in a coincidence does not affect the probability of a second detection, and the Akcasu/Stolle formulation, where it does. As with other measurements, the Akcasu/Stolle formulation significantly over predicts the k_{eff} value at low k_{eff} values. For example, at a calculated neutron multiplication factor of 0.455, the Akcasu/Stolle formulation gives a $k_{eff} = 0.585$, and the Pare/Mihalczo formulation gives a $k_{eff} = 0.450$ in agreement with calculations.

The benchmarks could be performed for directly measured quantities, such as the ratio of spectral densities, prompt neutron decay constants, count rates, rather than the neutron multiplication factors obtained from the ratio of spectral densities. Directly measured quantities will have lower uncertainties than inferred quantities because additional parameters to interpret the measured data have uncertainties, such as the neutron multiplication factor from the CSDNA measurements.

The experimental data recorded online need to be reevaluated. These experiments are summarized here to provide information so that at a later date, researchers could perform the required uncertainty and calculational analyses and documentation to use these data for an International Criticality Safety Benchmark Program (ICSBEP) or Nuclear Energy Agency (NEA) benchmark. The data from the measurements are available from ORNL Records Management Services Department, and the ORNL logbook is available from John Bess at Idaho National Laboratory.

ACKNOWLEDGMENTS

The work of E. B. Johnson in handling the uranyl nitrate solution, E. D. Blakeman in calculational support, and W. T. King in the performance and analysis of the data is acknowledged.

REFERENCES

1. J. T. Mihalczo and V. K. Paré, “Theory of Correlation Measurement in Time and Frequency Domains with ^{252}Cf,” *Ann. Nucl. Energy*, **2**, 97–105 (1975). [OSTI #4243449]
2. J. T. Mihalczo, W. T. King, E. B. Johnson, and E. D. Blakeman, “Subcriticality Measurements for a Fuel Solution Tank with Changing Fuel Concentration using the CF-252-Source-Driven Noise Analysis,” Meeting of the American Nuclear Society, San Francisco, *Trans. Am. Nucl. Soc.* 45, 337–38 (1983).
3. John T. Mihalczo, “Critical and Subcritical NEA Benchmark Possibilities for Measurements at ORCEF and Other US DOE Facilities”, ORNL/TM-2019/1188 (June 2019)
4. ORNL Logbook: H00228-Solution Tanks-1983, Records Management Department, Oak Ridge National Laboratory and ICSBEP and Idaho National Laboratory
5. Records Management Department, Oak Ridge National Laboratory, ORNL-DWG QSK-GWA-830406
6. E.D. Blakeman and T. E. Valentine, “Unreflected High Enriched Uranyl Nitrate Subcritical Noise Measurements,” SUB_HEU_SOL_THERM-001, NEA/NSC/DOC/(95)03/II Volume II (2000).
7. E. D. Blakeman, “Subcritical Noise Measurements for Two Coaxial Cylindrical Tanks Containing 93.1 wt. % Uranyl Nitrate Solution,” SUB_HEU_SOL_THERM-002, NEA/NSC/DOC/(95)03/II Volume II (2008).
8. Records Management Department, Oak Ridge National Laboratory ORNL Drawing Q-5167-1
9. A. Z. Akcasu and A. Stolle, “Langevin Equation Approach to Reactor Noise Analysis: Stochastic Transport Equation,” *Nucl. Sci. Eng.* **113**, no. 1, 31–55 (1993).

10. J. T. Mihalczo and W. T. King, “Noise Equivalent Source for Frequency Domain Measurements from the Spontaneous Fission of ^{252}Cf,” *Trans. Am. Nucl. Soc.*, ANS Winter Meeting, Washington DC (Nov 16–21, 1986).
11. R. R. Spencer, R. Gwin, and R. Ingle, “A Measurement of the Average Number of Prompt Neutrons from Spontaneous Fission of Californium-252,” *Nucl. Sci. Eng.* 80, 603 (1982).
12. R. E. Uhrig, *Random Noise Techniques in Nuclear Reactor Systems*, The Ronald Press (January 1970).

APPENDIX A. MONTE CARLO MODEL OF THE CALIFORNIUM IONIZATION CHAMBER

A detailed Monte Carlo N-Particle (MCNP) model of the Cf ionization chamber used in these experiments was originally given in a previous International Nuclear Criticality Safety Benchmark Evaluation Program benchmark, SUB-HEU-SOL-THERM-002 [ref A.1]. For convenience, the sketch is given here in Figure A.1. The MCNP input files for this source configuration is given an appendix in this reference and would be useful for preparing and MCNP input file for calculations including the source configuration. This appendix has appeared in other ORNL reports [A.2 and A.3] where this type of californium source has been used.

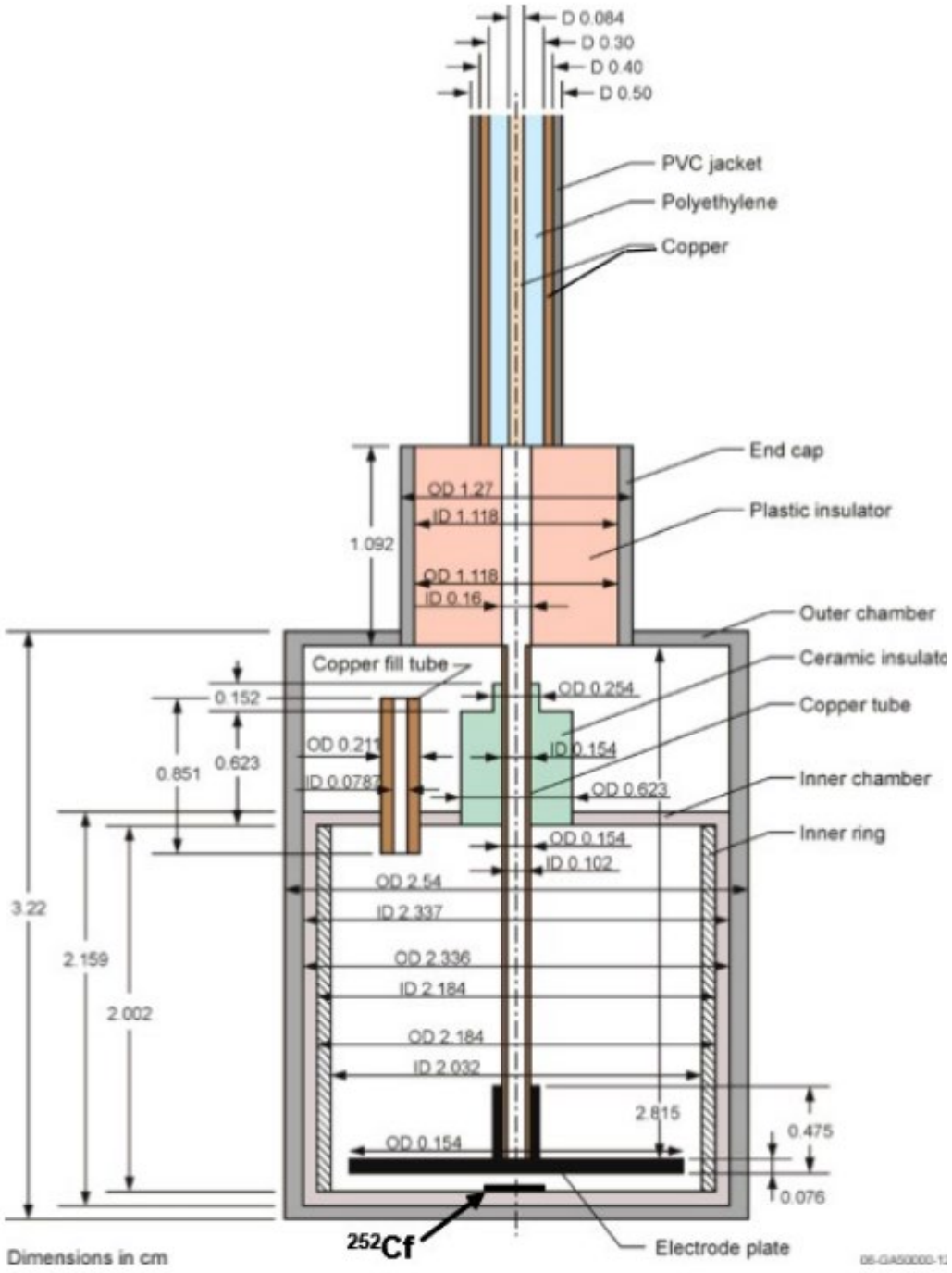

Figure A.1. MCNP model of the Cf source ionization chamber.

REFERENCES

A.1. Edward D. Blakeman, “Subcritical Noise Measurements for Two Coaxial Cylindrical Tanks Containing 93.1 % Uranyl Nitrate Solution” NEA/NSC/DOC/(95)03II, Volume II SUB-HEU-SOL-THERM-002 (2018).

A.2. John T. Mihalczo, “Critical and Californium Source-Driven Noise Analysis Subcritical Measurements with an Unreflected Cylindrical Tank of Mixed Uranium-Plutonium Nitrate Solution” ORNL/TM-2021/1606 (June 2022).
A.3. John T. Mihalczo, “Subcritical Californium Source-Driven Noise Analysis Measurements with Unreflected Uranium (93.15) Hydride” ORNL/TM-2021/1963 (June 2021).

APPENDIX B. RUN NUMBER WITH SOURCE DETECTOR LOCATIONS FOR VARIOUS SOLUTION CONCENGRATIONS

This appendix presents a list of all the experimental runs with detector and source locations prepared by two of the experimenters (W. T. King and J. T. Mihalczo) as the measurements progressed. The list of measurements with the source and detector locations is given in Table B.1 which is an image of Page 2 and following pages of the logbook.

Table B.1. List of a description of measurement for the solution tank with changing fissile concentration.

Noise analysis run	Solution concentration g U/ℓ	Source location (r, z, θ) (cm)	Detector type and location 2 Type	2 Location	3 Type	3 Location	Frequency range (kHz)	Remarks
AC	14.71	0,0 (a)	SCI	E	SCI	W	0.5	Central source, Li outside 180°
AD	14.71	OS,W,0 (b)	SCI	OS N	SCI	OS S	0.5	Source outside, Li outside 180°
AE	14.71	OS,W,0	SCI	SE	SCI	SW	0.5	Source outside, Li outside 120°
AF	14.71	0,0	He	15.2E	He	15.2W	0.5	Detector traverse, central source
AG	14.71	0,0	He	20.2E	He	15.2W	0.5	Detector traverse, central source
AH	14.71	0,0	He	25.4E	He	25.4W	0.5	Detector traverse, central source
AI	14.71	0,0	He	30.5E	He	30.5W	0.5	Detector traverse, central source
AJ	14.71	0,0	He	36.8E	He	36.8W	0.5	Detector traverse, central source
AK	14.71	0,0	He	25.4E	He	25.4W	0.5	Detector traverse, central source
AL	14.71	25.4S,0	He	7.6E	He	7.6W	0.5	Detector traverse, source at 25.4 cm
AM	14.71	25.4S,0	He	16.5E	He	16.5W	0.5	Detector traverse, source at 25.4 cm
AN	14.71	25.4S,0	He	25.4E	He	25.4W	0.5	Detector traverse, source at 25.4 cm
AO	14.71	25.4S,0	He	33.0E	He	33.0E	0.5	Detector traverse, source at 25.4 cm
AP	14.71	25.4S,0	He	25.4NW	HE	25.4NW	0.5	Detector traverse, source at 25.4 cm
AQ	14.71	25.4S,0	He	25.4NW	He	25.4NW	0.5	Detector traverse, source at 25.4 cm
AR	14.71	25.4S,0	He	33.0NW	He	33.0NW	0.5	Detector traverse, source at 25.4 cm

(a) 0, 0 means the source is at the center (r equals 0), and the z value equal 0 is at the vertical center of the solution
(b) OS,W,0 means outside against the radial surface, W means on the west side, and 0 means at the vertical center of the solution.
For all measurements with the source outside, the CF-19 source was used, and for measurements with the source in the solution, Cf-20 in a Lexan tube was used.

Noise analysis run	Solution concentration g U/ℓ	Source location (r, z, θ) (cm)	Detector type and location 2 Type	2 Location	3 Type	3 Location	Frequency range (kHz)	Remarks
AS	14.71	25.4S,0	He	15.2NW	He	16.5NW	0.5	Detector traverse, source at 25.4 cm
AT	14.71	25.4S,0	He	33.0E	He	33.0W	0.5	Detector traverse, source at 25.4 cm
AU	14.71	36.8S, 36.8N,0	He	36.8E	He	36.8W	0.5	Two sources
AV	14.71	17.1S, 17.1N,0	He	25.4E	He	25.4W	0.5	Two sources
AW	14.71	0,0	He	7.6E	He	7.6W	0.5	Central source, detector traverse
AX	14.71	25.4S,0	He	12.1E	He	12.1W	0.5	Detector traverse, source at 25.4 cm
AY	14.71	19.0E,0	He	19.0N	He	19.0S	0.5	
AZ	14.71	0,19.0	He	20.3E	He	20.3W	0.5	Axial modes
BA	14.71	0,19.0	He	20.3E, -19.0	He	20.3W, -19.0	0.5	Axial modes
BB	14.71	0,19.0	He	20.3E -19.0	He	20.3W, 19.0	0.5	Axial modes
BC	14.71	0,19.0	He	20.3, -19.0	He	20.3W, 19.0	0.5	Axial modes
BD	14.71	1.9,+19.0 1.9,-19.0	He	20.3E	He	20.3W	0.5	Two sources, axial modes
BE	14.71	1.9,+19.0 1.9,-19.0	He	20.3E	He	22.9W	0.5	Two sources, axial modes
BF	14.71	1.9,-+19.0 1.9,-19.0	He	20.3E	He	22.9W	0.5	Two sources, axial modes
BG	14.71	1.9,+19.0 1.9,-19.0	He	20.3E	He	20.3W	0.5	Two sources, axial modes
BH	14.71	0,0	SCI(5)	OS/S	SCI(5)	OS N	0.5	Scintillators outside
BI	14.71	36.8,0,0	He	12.1E	He	12.1W	0.5	Source traverse
BJ	14.71	17.8,0,0	He	12.1E	He	12.1W	0.5	Source traverse
BK	14.71	10.8,0,0	He	12.1E	He	12.1W	0.5	Source traverse
BL	14.71	31.8,0,0	He	12.1E	He	12.1W	0.5	Source traverse
BM	14.71	5.1,0,0	He	12.1E	He	12.1W	0.5	Source traverse
BN	14.71	36.8S,0	SCI(5)	OS E	SCI(5)	OS W	0.5	Scintillators
BO	14.71	0,+38.1,0	SCI(5)	OS E	SCI(5)	OS W	0.5	Source on top
BP	14.71	36.8E,0	SCI(5)	OS 243°	SCI(5)	OS 297°	0.5	Source at edge, θ traverse of detector
BQ	14.71	36.8E,0	SCI(5)	OS 210°	SCI	OS 330°	0.5	Azimuthal det traverse
BR	14.71	36.8E,0	SCI(5)	OS SE,0	SCI	OS NW	0.5	Azimuthal det traverse
BS	14.71	36.8E,0	SCI(5)	OS SE,0	SCI	OS NW	0.5	Azimuthal det traverse
BT	14.71	36.8E,0	SCI(5)	OS SE,0	SCI	OS NE	0.5	Azimuthal det traverse

Noise analysis run	Solution concentration g U/ℓ	Source location (r, z, θ) (cm)	Detector type and location 2 Type	2 Location	3 Type	3 Location	Frequency range (kHz)	Remarks
BU	14.71	0,0	SCI(5)	OS SE,0	SCI	OS NE	0.5	Source center
BV	14.71	0,38.1	SCI(5)	OS SE,0	SCI	OS NE	0.5	Source top
BW	14.71	36.8W,0	SCI(5)	OS SE,0	SCI	OS NE	0.5	Det 120°
BX	14.71	0,0	SCI(5)	OS S,19.0	SCI	OS S,-19.0	0.5	Axial modes
BY	14.71	0,38.1	SCI(5)	OS S,19.0	SCI	OS S,-19.0	0.5	Source on top
BZ	14.71	OS N,0	SCI(5)	OS S,19.0	SCI	OS S,-19.0	0.5	Source outside tank
CA	14.71	OS N,0	SCI(5)	OS S,0	SCI	OS N,0	0.5	4" SS 316 - on det
CB	14.71	0,0	SCI(5)	OS S,0	SCI	OS N,0	0.5	No steel
CC	14.71	OS W,0	SCI(5)	OS S,0	SCI	OS N,0	0.5	Cf 16
CE	14.71	OS E,0	SCI(5)	OS S,0	SCI	OS N,0	0.5	Cf 16 with 19.2 cm steel
CF	13.28	0,0	SCI(5)	OS S,0	SCI	OS N,0	0.5	Cf 19
CG	13.28	0,0	SCI(5)	OS S,0	SCI	OS N,0	1.0	
CH	13.28	36.8W,0	SCI(5)	OS S,0	SCI	OS N,0	1.0	
CI	13.28	0,0	SCI(5)	OS 150,0	SCI	OS 30,0	1.0	Det 120° apart
CJ	13.28	0,0	SCI(5)	OS 135,0	SCI	OS NE,0	1.0	Detectors 120° apart
CK	13.28	0,38.1	SCI(5)	OS 135,0	SCI	OS NE,0	1.0	Source top 90° det

Noise analysis run	Solution concentration g U/ℓ	Source location (r, z, θ) (cm)	Detector type and location 2 Type	2 Location	3 Type	3 Location	Frequency range (kHz)	Remarks
CL	13.28	0,38.1	SCI(5)	OS 305,0	SCI	OS SE,0	1.0	Source top 90° det
CM	13.28	36.8E,0	SCI(5)	OS 305,0	SCI	OS SE,0	1.0	Source east
CN	13.28	25.4E,0	He	12.1N,0	He	12.1S,0	1.0	Source traverse
CO	13.28	17.8E,0	He	12.1N,0	He	12.1S,0	1.0	Source traverse
CP	13.28	0,0	He	36.8E,0	He	36.8W,0	1.0	" "
CQ	13.28	0,0	He	17.8 ,0	He	17.8 ,0	1.0	" "
CR	13.84	0,0	He	36.8 ,0	He	36.8 ,0	1.0	" "
CS	13.84	12.8E,0	He	12.1N,0	He	12.1S,0	1.0	" "
CT	13.84	25.4E,0	He	12.1N,0	He	12.1S,0	1.0	" "
CU	13.84	OS E,0	SCI(5)	OS-330,0	SCI	OS-210,0	1.0	120°
CV	13.84	00,0	~~He~~ SCI(5)	OS-SE,0	~~SCI~~ ~~He~~	OS-315°,0	1.0	
CW	13.84	0,38.1	~~He~~ SCI(5)	OS-SE,0	SCI ~~He~~	OS-315°,0	1.0	
CX	13.84		SCI(5)	OS-SE,0	SCI	OS-315°,0	1.0	
CY	13.84	0,0	SCI(5)	OS-SE,0	SCI(5)	OS NW,0	1.0	
CZ	13.84	0,0	SCI(5)	OS SE,0	SCI(5)	OS NE,0	1.0	
DA	13.84	0,38.1	SCI(5)	OS SE,0	SCI(5)	OS NE,0	1.0	

Noise analysis run	Solution concentration g U/ℓ	Source location (r, z, θ) (cm)	Detector type and location 2 Type	2 Location	3 Type	3 Location	Frequency range (kHz)	Remarks
DB	13.84	36.8W,0	SCI(5)	OS N,0	SCI(5)	OS S,0	1.0	
DC	13.84	0,0	He	17.8N,0	He	17.8S,0	1.0	
DD	12.89	0,0	SCI(5)	OS N,0	SCI(5)	OS S,0	1.0	
DE	12.89	0,38.1	SCI(5)	OS S,0	SCI(5)	OS N,0	1.0	Source on top
DF	12.89	0,0	He	17.8N,0	He	17.8S,0	1.0	
DG	12.89	0,0	He	17.8N,W,0	He	17.8 S,E,0	1.0	2 counters
DH	12.89	0,0	He	17.8 E,W,0	He	17.8 N,S,0	1.0	2 counters
DI	12.89	36.8W,0	SCI	OS S	SCI	OS N	1.0	
DJ	12.89	17.8E,0	He	12.1S	He	12.1N	1.0	
DK	12.89	0,0	SCI	OS SE	SCI	OS NW	1.0	
DL	12.89	36.8,E,0	SCI	OS SE	SCI	OS NW	1.0	
DM	12.89	0,0	2-SCI	OS E,W	2-SCI	OS N,W	1.0	2 scintillators
DN	12.89	0,0	2-SCI	OS E,W	2-SCI	OS N,S	1.0	
DO	11.88	0,0	SCI	OS SE	SCI	OS NW	1.0	New concentration
DP	11.88	36.8W,0	SCI	OS SE	SCI	OS NW	1.0	
DQ	11.88	36.8 E,0	SCI	OS N	SCI	OS S	1.0	

REFERENCES

B.1. ORNL notebook H00228 ORCEF Solution Tanks-1983, experimental logbook for the measurements, Records Management Services Department of ORNL and the International Criticality Safety Benchmark Evaluation Program at Idaho National Laboratory.

APPENDIX C. ONLINE RATIOS OF SPECTRAL DENSITIES AND COHERENCE VALUES FOR ALL MEASUREMENTS

The cross and auto correlation functions are combined in a ratio of spectral densities, G_{S1}* G_{S2}/ Gss G_{23}, where * means complex conjugation. The ratio is constant at low frequencies and averages over the frequency range where it is constant and used to obtain the neutron multiplication factor using a point kinetics model to infer the neutron multiplication factor, k_{eff}. The californium source-driven noise analysis online results for the measurement of the ratio of spectral densities at low frequency are given in Table C.1. Also given in this appendix are the values of the coherence between detectors. The coherence between two detectors $(\gamma_{12})^2$ is (G^*_{12} times G_{12}) / (G_{11} times G_{22}). The values of $(\gamma_{s1})^2$, $(\gamma_{s2})^2$, and $(\gamma_{23})^2$ are also given in Table C.1. For low coherence values, the coherence is the amount of common information in two signals. This table was prepared by the author of this report from the Experimental log book [C.1.]

Table C.1. Online measurement results for coherences and ratio of spectral densities.

Run number	Logbook page number	Coherence source-detector 1 (10^{-3})	Coherence source-detector 2 (10^{-3})	Coherence between detectors (1×10^{-3})	Ratio of spectral densities
AC(He)	20	7	7	2	0.19
AD	21	Not recorded	Not recorded	Not recorded	0.016
AE	22	Not recorded	Not recorded	Not recorded	0.0093
AF	24	54	55	40	0.287
AG	25	26	30	30	0.161
AI	27	19	18	10	0.18
AJ	28	6.5	6.5	1.5	0.18
AK	29	28	27	20	0.20
AL	30	22	22	8.5	0.077
AM	31	18	18	9.5	0.085
AN	34	10	12	18	0.08
AO	35	25	26	5.5	0.78
AP	37	8.5	9	27	0.05
AQ	39	8	9	27	0.05
AR	40	5	5	8	0.05
AS	41	13	16	7	0.055
AT	42	7.2	6.3	5.5	0.08
AU	43	0.8	0.8	1.6	0.024
AV	44	86	85	50	0.135
AW	45	96	95	50	0.096
AX	46	Not recorded	Not recorded	Not recorded	0.09
AY	47	24	25	38	0.135
AZ	48	Not recorded	Not recorded	Not recorded	Not recorded
BA	49	12	14	36	0.064
BB	50	36	39	20	0.26
BC	51	12	40	12	0.174
BD	53	24	23	30	0.132
BE	54	20	18	18	0.144

Table C-1. Online measurement results for coherences and ratio of spectral densities.

Run number	Logbook page number	Coherence source-detector 1 (10^{-3})	Coherence source-detector 2 (10^{-3})	Coherence between detectors (1×10^{-3})	Ratio of spectral densities
BF	55	25	22	10	Not recorded
BG	56	20	21	20	0.147
BH(SCI)	61	40	27	32	0.174
BI	62	6	6	7	0.022
BJ	63	36	35	63	0.14
BK	64	55	55	60	0.21
BL	65	12	12	70	0.045
BN	67	4	3.5	15	0.034
BO	68	3.4	3.2	13	0.024
BP	71	3	2	4	0.011
BQ	72	3.9	2.3	2.6	0.018
BR	74	10	8	10	0.078
BS	75	16	2.8	13	0.52
BT	76	16	12	16	0.11
BU	77	35	28	40	0.147
BV	78	3	2.5	14	0.0219
BW	79	3.2	2.1	24	0.015
BX	80	27	21	32	0.132
BY	81	5	5	12	0.024
BZ	82	1.6	1.6	1.9	0.122
CA	83	4	38	0.5	0.155
CB	84	7.5	4.5	1.5	0.158
CF	91	32	24	14	0.251
CG	92	30	24	13	0.248
CH	93	3.8	2.4	3.4	0.058
CI	95	32	24	16	0.224
CJ	96	31.5	27	20	0.192
CK	97	3	1.6	2.8	0.034
CL	98	2.8	2	3	0.045
CM	99	17	1	2.5	0.0764
CO	101	Not recorded	Not recorded	Not recorded	0.203
CP	102	4	5.2	4	0.24
CQ	103	40	40	13	0.34
CR	105	5	6	6	0.218
CS	106	32	31	32	0.171
CT	107	17	17	33	0.096
CU	108	2.1	1.6	6	0.0238
CV	109	34	27	21	0.22
CW	112	3.2	2	4	0.0386

Table C-1. Online measurement results for coherences and ratio of spectral densities.

Run number	Logbook page number	Coherence source-detector 1 (10^{-3})	Coherence source-detector 2 (10^{-3})	Coherence between detectors (1×10^{-3})	Ratio of spectral densities
CX	113	2.4	1.2	6	0.068
CY(He)	116	40.5	38	35	0.216
CZ	117	36	36	38	0.177
DA	118	3.8	3.6	13	0.032
DB	119	4.4	5.2	12	0.0468
DC	120	45	46	20	0.308
DD NC	123	30	30	13	0.286
DE	124	3.2	2.9	3	0.0676
DF	126	36	40	9	0.38
DG	127	63	63	32	0.35
DH	128	65	64	41	0.31
DI	129	3.6	3.6	3	0.062
DJ	190	24	36	16	0.1887
DK (SCI)	131	30	30	20	0.2144
DL	132	1.2	1.6	2.6	0.055
DM	133	54	54	46	0.243
DN	134	54	54	60	0.219
DO	137	24	24	6	0.319
DP	138	0.8	216	0.8	0.125
DQ	140	3.2	3.2	1.4	0.085
DR	141	12	14	9	0.133
DS	142	2.4	2.8	1	0.077
DT	143	24	23	10	0.245
DU	144	47	43	44	0.2
DV	145	45	44	18	0.32
DW	146	1.2	1.2	1	.036
DX	147	46	46	39	0.228
DY	148	42	42	20	0.306
DZ	149	45	45	26	0.278
EA	150	47	45	35	0.252
EB	151	3.7	3.6	4	0.524
EC	152	3.3	3.3	1.6	0.0875
ED	153	9	8.5	0.6	0.0418
EE	154	3.6	4.6	3.2	0.0711
EF	155	4.2	3.6	1.5	0.101
EG	156	24	24	9	0.253
EH	157	1.6	1.6	1.8	0.385
EI	158	1.3	1.3	2	0.32
EJ	159	22	24	9.4	0.23

Table C-1. Online measurement results for coherences and ratio of spectral densities.

Run number	Logbook page number	Coherence source-detector 1 (10^{-3})	Coherence source-detector 2 (10^{-3})	Coherence between detectors (1×10^{-3})	Ratio of spectral densities
EK	160	12	12	8	0.123
EL	162	21	19	27	0.0385
EM	163	1.2	1.6	0.2	0.0906
EN	164	20	22	7	0.240
EO	166	9	11	0.8	0.35
EP	167	34	33	9	0.387
EQ	168	20	19	25	0.293
ER	169	2.2	3.2	2.5	0.116
ES	170	12	11	1.7	0.314
ET	171	12	11	16	0.321
EU	172	1.8	1.6	0.7	0.063
EV	175	27	26	5	0.417
EW	176	1.8	2.2	0.36	0.12
EX	177	15	15	3.2	0.266
EY	178	6	6.6	2.4	0.14
FA	180	2.9	3.0	0.4	0.157
FB	181	1	1	1.9	0.071
FC	182	2	1	1.2	0.412
FD	183	9,5	9.5	0.8	0.343
FE	184	8	8	0.9?	0.3
FF	187	22	22	22	0.456
FG	188	24	33	3.6	0.467
FH	189	1.6	3.0	1.6	0.156
FI	190	2.7	4.5	0.24	0.194
FJ NC	193	18	25	1.6	0.542
FK	194	1.4	2.3	0.12	0.205
FL	195	2	2.8	0.1	0.249
FM	196	0.7	1	0.4	0.1124
FN	200	16	20	1	0.578
FO	201	14	23	0.34	0.31
FP	202	0.9	1.6	0.2	0.232
FQ	206	4.5	4.2	0.7	0.502
FR		8.5	9	0.39	0.413
FS	213	1.5	1.8	0.8	0.601
FT	214	Not recorded	Not recorded	Not recorded	Not Recorded
FU	216	1.2	3.5	0.4	0.36
FV	217	0.95	2.5	0.2	0.29
FW	221	8	14	0.2	0.65
FX SCI	223	2	15	0.7	0.697

Table C-1. Online measurement results for coherences and ratio of spectral densities.

Run number	Logbook page number	Coherence source-detector 1 (10^{-3})	Coherence source-detector 2 (10^{-3})	Coherence between detectors (1×10^{-3})	Ratio of spectral densities
FY	224	Not recorded	Not recorded	Not recorded	Not Recorded
FZ	226	2	1.7	0.22	0.375
GA SCI	230	17	13	0.4	0.744
GB	231	2.5	2.2	0.2	0.454
GC	232	4.2	3.0	0.055	0.499
GD SCI	238	15	14	0.3	0.816
GE	240	2.7	3.0	0.5	0.499
GF	241	Not recorded	Not recorded	Not recorded	Not recorded
GG	242	16	30	1	0.825
GH	245	15	13	0.48	0.889
GI	246	15	12.5	0.22	0.832
GJ	247	1.5	1.4	3.6	0.836
GK	248	2.5	2	0.2	0.47
GL SCI	252	1.4	0.9	0.14	0.862

REFERENCES

C.1. ORNL notebook H00228 ORCEF Solution Tanks-1983, experimental logbook for the measurements, Records Management Services Department of ORNL and the International Criticality Safety Benchmark Evaluation Program at Idaho National Laboratory.

APPENDIX D. CALIFORNIUM SOURCE-DRIVEN NOISE-ANALYSIS

This appendix appears in full in previous ORNL reports [D.1 and D.2] and is included here for convenience.

D.1 BACKGROUND

This appendix presents a review of the source noise analysis method and its original development and present status. This method has its origins in time correlation function measurement, which is the time distribution of counts in one detector with respect to a previous count in the same or another detector. This was first suggested by Bruno Rossi during the Manhattan Project and is known as the two- and one-detector Rossi-α measurement [D.3]. Because it requires two counts, the measurement depends on the square of the detection efficiency. In 1968, californium was deposited on one plate of a parallel plate ionization chamber, and its spontaneous fission provided a timing signal as to when neutrons were emitted. Therefore, the use of californium in this way provided the basis for a randomly pulsed neutron source [D.4], which was used to measure the time distribution of counts in a detector with respect to a count in the californium ionization chamber. This measurement acquired data much faster than the Rossi-α because it depended on the detection efficiency and not its square, and the efficiency for counting spontaneous fission of californium was near 100%.

In 1975, the author joined the research group doing reactor noise [D.5] measurements in the frequency domain rather than the time domain. These measurements had some advantages when the fission rates were so high that fission chains overlapped and could not be distinguished in the time domain. The auto and cross power spectral densities in the frequency domain are just the Fourier transform of the autocorrelation function and the cross correlation functions in the time domain. These frequency domain measurements had been developed for reactors operating at high power. This method was designated as the californium source-driven noise analysis and was used from about 1975 to 2000 to measure the subcriticality at eight US Department of Energy facilities [D.6].

In these measurements, the californium source ionization chamber and two detectors were used. This technique measured a ratio of spectral densities that was independent of detection efficiency and thus avoided the problems of neutron source multiplication methods [D.7], which had been used for decades to monitor the approach to critical in critical facilities and in the initial startup of reactors. In about 1984, the first time domain measurements were performed with nuclear weapons/components of highly enriched uranium metal using a time-tagged ionization chamber. Through the 1980s and 1990s, the Nuclear Materials Identification System (NMIS) was developed. The number of detectors initially increased to five. Since the fission chain decay was so rapid in these systems and these systems were subcritical, most of the analysis used time domain measurements in which smaller californium sources were used. However, the frequency analysis result capability was maintained in the NMIS software. Mihalczo, Mullens, Mattingly, and Valentine (2000) provide a physical description of the signatures acquired by NMIS [D.8]. The use of a time-tagged californium ionization chamber with its isotropic emission of neutrons created background problems for some measurements. In 2004, some analysis by James Mullens [D.9] indicated that with a time- and directionally tagged neutron generator, the NMIS system could be expanded to perform neutron imaging. The time and directional tagging were accomplished by detecting the alpha particle from the deuterium-tritium reaction, which is emitted ~180° from the neutron emission [D.10]. The NMIS software for acquiring (DAUI) and interpreting (IDAS) data was modified to multiplex signals depending on their width. The NMIS capability at that time was 10 input channels capable of eight or more detectors per channel. This allowed using a row of 16 alpha pixels to define a fan beam of neutron cones, each with a separate direction and using a radial arc of 32 detectors that can be used for imaging. This imaging work was originally supported by the Y-12 National Security complex and later by the US Department of Energy Office of Nuclear Verification. Also, NMIS employed eight additional

large detectors that could be used for active and passive time correlation measurements. The US Department of Energy Office of Nuclear Verification then supported a friendlier, treaty-usable system designated as the Fieldable Nuclear Material Identification System [D.11]. In 2006, a more advanced, highly pixelated system was developed by Paul Hausladen and coworkers [D.12].

D.2 CALIFORNIUM SOURCE-DRIVEN NOISE ANALYSIS METHOD

This method was originally developed in 1975 for subcriticality determinations for three detectors—a time-tagged californium source and two detectors. The development of the equations for this method is given in the literature [D.13].

D.3 NOISE EQUIVALENT SOURCE

The point kinetics equations presented use the Oak Ridge National Laboratory (ORNL) version of the noise equivalent source. An alternate version of the noise equivalent source was developed by Akcasu and others [D.14]. This latter version has a better theoretical foundation. However, for highly subcritical systems, its use results in overestimation of the neutron multiplication. In 1990, researchers at Knolls Atomic Power Laboratory (KAPL) performed a completely independent analysis and compared the results of interpretation of measurements with both methods [D.15]. Basically, at neutron multiplication factors above 0.80, both point kinetics methods give similar results, but not below 0.80. This will be illustrated in subsequent sections of this appendix.

D.4 HIGHLY ENRICHED URANYL NITRATE SOLUTION TANK EXPERIMENT

A photograph of the tank that contained uranyl nitrate solution is given in Figure B.1. The measurements were performed with external plastic scintillation detectors detecting leakage neutrons above 1 MeV and gamma rays and external ^{3}He proportional counters detecting the lower energy spectrum of leakage neutrons. These results for measurements as a function of solution height, which are a ratio of spectral densities that can be interpreted to obtain the neutron multiplication factor, are shown in Table D.1 and in Figures D.2 and D.3. The results show the agreement with calculated neutron multiplication factors.

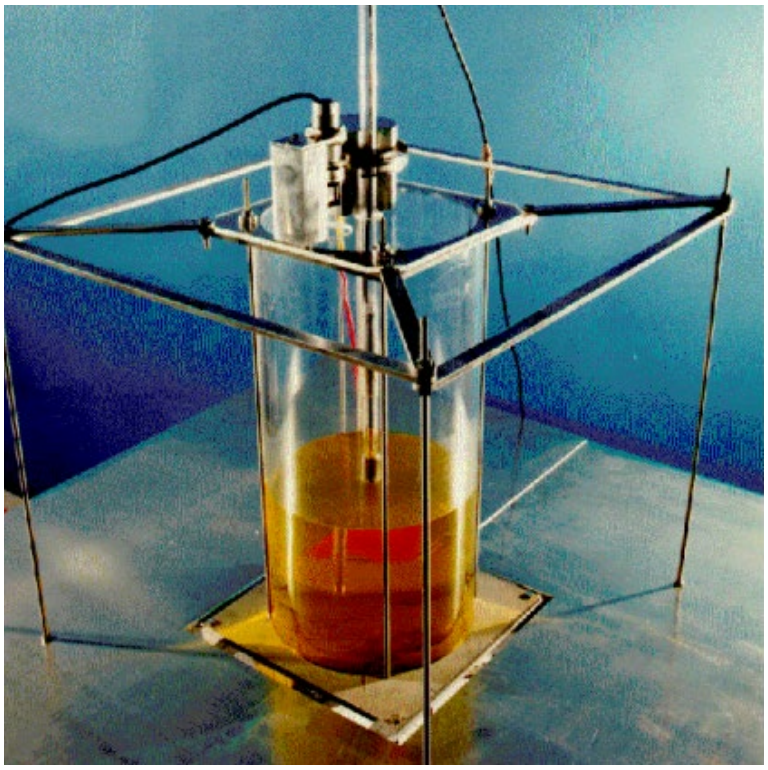

Figure D.1. Highly enriched uranyl nitrate solution tank without external detectors and the californium source at the top of the solution (solution color distorted from actual yellow by red tape on the table behind the tank).

Although the source is at the bottom of the solution, a location where point kinetics should not be valid, most of the coincidences come from fission chains with large number of fissions that are distributed spatially like the fundamental mode.

Table D.1. Measured ratios of spectral densities at low frequencies and neutron multiplication factors from static measurement with the source at the bottom of the solution.

Solution Height (cm)	Ratio of Spectral Densities[a]		Neutron Multiplication Factors, k_{eff}[b]		Number of Data Blocks (10^3)
	^{3}He Detectors (10^{-4})	Scintillators (10^{-4})	^{3}He Detectors	Scintillators	
29.2	453 ± 12 (5)	436 ± 5 (2)	0.952 ± 0.002	0.954 ± 0.001	20
25.8	767 ± 40 (5)	774 ± 20 (2)	0.924 ± 0.005	0.923 ± 0.003	20
20.3	1590 ± 20 (5)	1616 ± 10 (6)	0.853 ± 0.005	0.850 ± 0.005	20
15.3	2896 ± 90 (5)	2843 ± 10 (10)	0.732 ± 0.015	0.738 ± 0.010	40
10.1	4508 ± 90 (5)	4477 ± 60 (10)	0.535 ± 0.030	0.540 ± 0.027	20
9.8	---	4723 ± 60 (10)	---	0.505 ± 0.030	7
9.0	---	4960 ± 60 (10)	---	0.472 ± 0.035	100
7.5	---	5293 ± 210 (10)	---	0.414 ± 0.055	40
6.5	---	5650 ± 60 (10)	---	0.346 ± 0.049	60
5.7	---	5943 ± 360 (10)	---	0.278 ± 0.097	55

[a]Values in parentheses are the upper limit of the frequency range in kilohertz over which the ration was averaged. The precision given is one standard deviation of the mean. Uncertainties in the neutron multiplication factor are from the statistical precision of the ratio of spectral densities and the uncertainties in the parameters required to infer the neutron multiplication factor

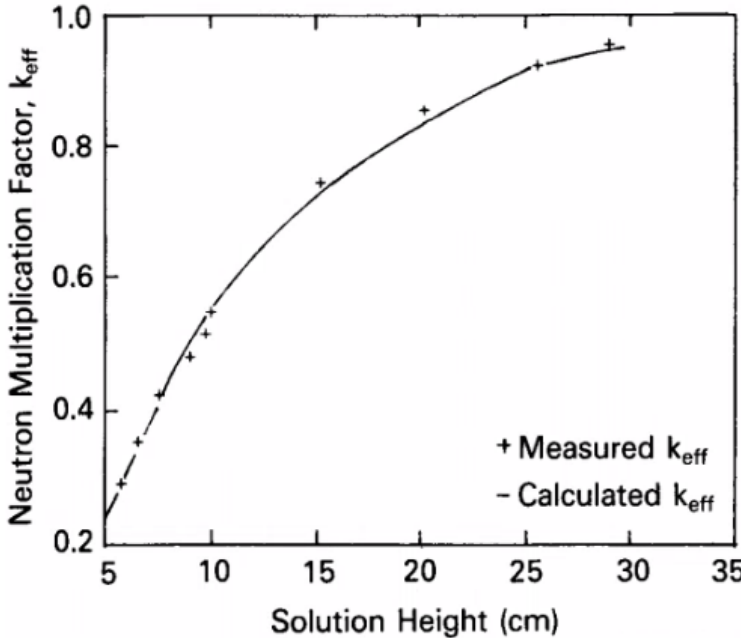

Figure D.2. Comparison of neutron multiplication factors obtained for the author's formulation of detection effects from static measurement with two ^{3}He proportional counters adjacent to the tank detecting leakage neutrons and with the source at the bottom of the tank.

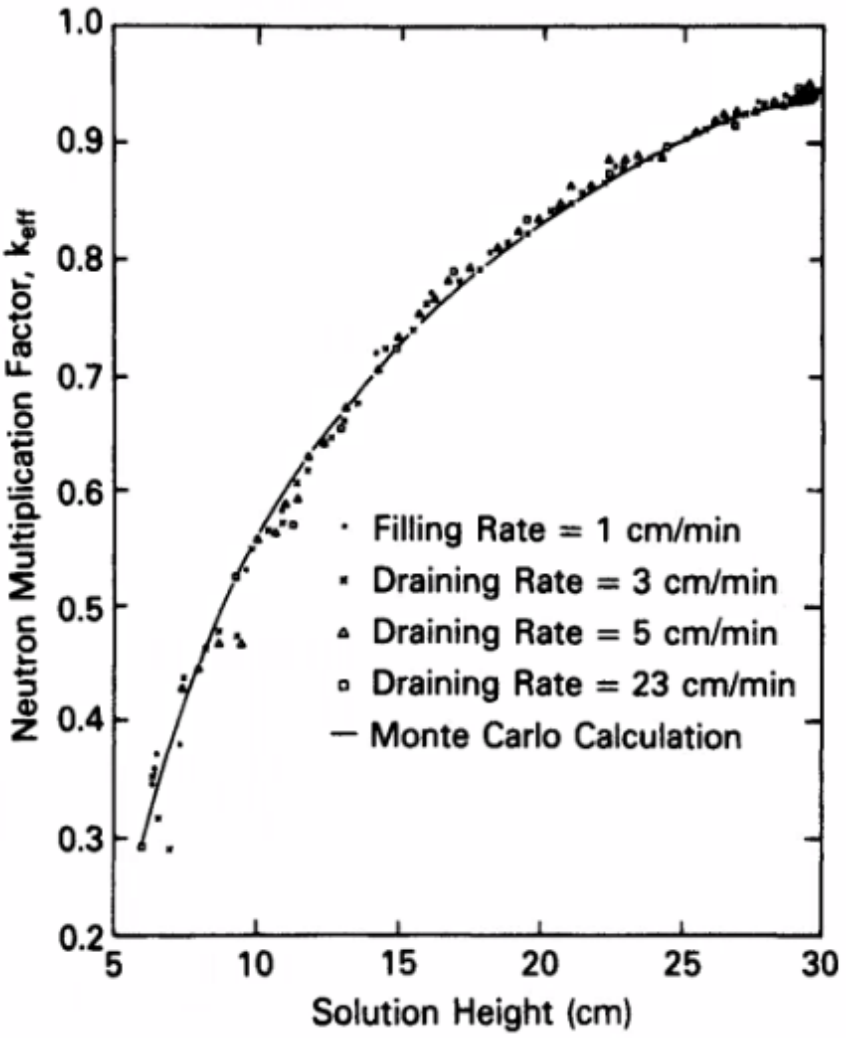

Figure D.3. Comparison of neutron multiplication factors obtained for the author's formulation of detection effects from dynamic measurement with two fast plastic scintillators adjacent to the tank detecting leakage neutrons and gamma rays and the californium source at the bottom of the tank with calculations.

Notably, the measured ratio is the same as predicted by the theory for the ^{3}He proportional counters detecting lower-energy neutron spectrum neutrons and fast plastic scintillators detecting gamma rays and fast neutrons. Both these systems are detecting leakage neutron, and the scintillators are also detecting gamma rays. In fact, calculations have shown that most plastic scintillator coincidences involve only one neutron and gamma rays (private communication report from P. M. Keates, UK, to J. Mihalczo, Oak Ridge National Laboratory, 2019, available from John Mihalczo).

The measured and the calculated neutron multiplication factors are in excellent agreement. The neutron multiplication factors from the dynamic measurement as the tank was drained with the fast plastic scintillators and the californium source on the bottom of the tank are compared with calculations in Figure D.3. For all draining rates, the measured neutron multiplication factors agree, and they also agree with the calculations.

D.5 INTERPRETATIONS BY KNOLLS ATOMIC POWER LABORATORY USING BOTH POINT KINETICS FORMULATIONS AND COMPARISON WITH CALCULATIONS

A report by researchers at KAPL [D.15] also evaluated the ratio of spectral densities to obtain, using both the author's point kinetics formulations and the Akcasu/Stolle formulation independent of ORNL (i.e., all the necessary parameters to infer the neutron multiplication factor were obtained by Sutton and coauthors independent of ORNL for the ORNL interpretation). KAPL researchers also calculated the neutron multiplication factor by the KAPL Monte Carlo code (RACER) and compared with the two different point kinetics formulations of interpretation of the ratio of spectral densities. Their calculated neutron multiplication factors agreed with their interpretation of the ratio of spectral densities using the ORNL formulation. The interpretation using the formulation from KAPL and others gave neutron multiplication factors that were much higher than those from the author's interpretation at the low neutron multiplication factor values. These comparisons are presented in the Figure D.4. At a solution height of 4 in., the Pare/Mihalczo formulation gave a k_{eff} of 0.56 compared with 0.69 for the KAPL interpretation using Sutton's formulation. RACER Monte Carlo–calculated neutron multiplication factors agree with the author's formulation of the noise equivalent source formulation. At neutron multiplication factors above 0.85, the inferred neutron multiplication from both point kinetics formulations is essentially the same.

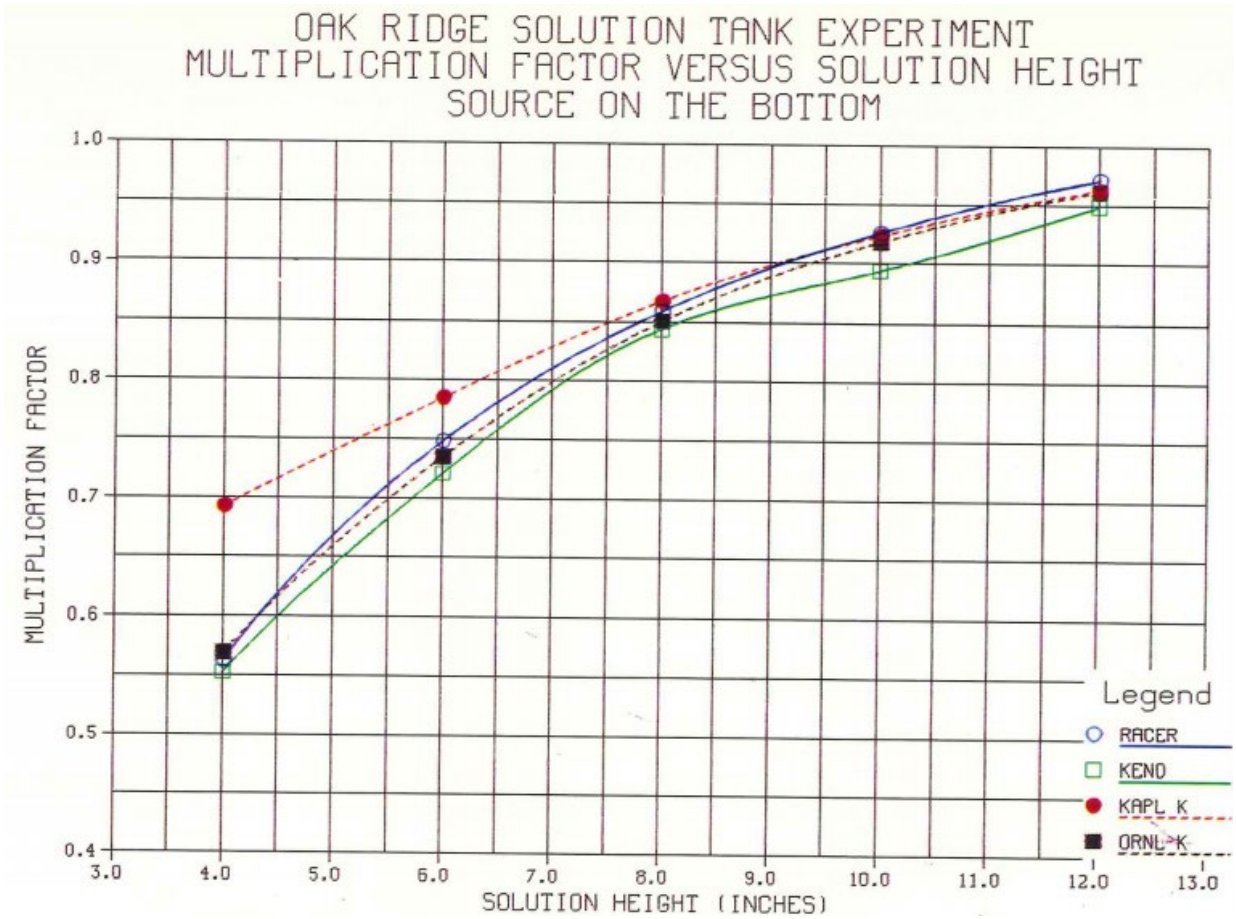

Figure D.4. Comparison of neutron multiplication factors from RACER Monte Carlo calculations with the two formulations. (Red circles are KAPL interpretation using the Akcasu/Stolle formulation, and black boxes are KAPL'S formulation using the author's formulation.)

At low neutron multiplication factors, the interpretation using the KAPL formulation gives results that do not agree with the RACER calculations. For a solution height of 4 in., the Akcasu/Stolle formulation gives a neutron multiplication factor of 0.69, and the RACER Monte Carlo calculation gives 0.56. The disagreement increases as the neutron multiplication decreases and starts below the k_{eff} of 0.85.

A more general model has been used to determine the neutron multiplication factor from the measured results. The Monte Carlo method can be used to directly calculate the ratio of spectral densities and its uncertainty. This avoids the use of point kinetics and replaces it with a very general method that does not have the limitations of the point kinetics model. Some examples of this use of the more general model are given in Nuclear Energy Agency criticality safety benchmarks SUB-HEU-SOL-THERM-001 and SUB-HEU-Sol-THERM-002 [D.16, D.17].

REFERENCES

D.1. John T. Mihalczo, "Critical and Californium Source-Driven Noise Analysis Subcritical Measurements with an Unreflected Cylindrical Tank of Mixed Uranium-Plutonium Nitrate Solution" ORNL/TM-2021/1606 (June 2022).

D.2. John T. Mihalczo, "Subcritical Californium Source-Driven Noise Analysis Measurements with Unreflected Uranium (93.15) Hydride" ORNL/TM-2021/1963 (June 2021)

D.3. John D. Orndoff, "Prompt Neutron Periods of Metal Critical Assemblies," *Nuc. Sci. Eng.*, **2**, no. 4, 450–460 (1957).

D.4. J. T. Mihalczo, "The Use of Californium-252 as a Randomly Pulsed Neutron Source for Prompt Neutron Decay Measurements," *Nucl. Sci. Eng.*, **53**, no. 4, 393–414 (1974).

D.5. J. T. Mihalczo and V. K. Paré, "Theory of Correlation Measurement in Time and Frequency Domains with ^{252}Cf," *Ann. Nucl. Energy*, **2**, 97–105 (1975). [OSTI #4243449]

D.6. V. K. Paré and J. T. Mihalczo, "Reactivity from Power Spectral Density Measurements with Californium-252," *Nucl. Sci. Eng.*, **56**, no. 2, 213–218 (1975).

D.7. J. T. Mihalczo, "A Review of Methods for Treatment of Source Effects in the Modified Source Multiplication Method for Monitoring the Reactivity in Refueling the CRBR," ORNL-5568, Union Carbide Corp. Nuclear Division, Oak Ridge National Laboratory, September 1979. [OSTI #5984287]

D.8. J. T. Mihalczo, J.A. Mullens, J. K. Mattingly, and T. E. Valentine, "Physical Description on Nuclear Materials Identification System (NMIS) Signatures," *Nucl. Instrum. Methods Phys. Res., Sect. A*, **450**, nos. 2–3), 531–555 (Amsterdam Elsevier Science BV) (2000).

D.9. J. A. Mullens, J. T. Mihalczo, and P. Bingham, "Neutron and Gamma Ray Imaging for Nuclear Materials Identification", Proc. of INMM 45th Annual Meeting, Northbrook, Il, (July 2004).

D.10. D. Koltick, S. Kane, J. Mihalczo, S. McConchie, E. Mace, and M. Lvovsky, "Production of an Associated Particle Neutron Generator with ZnO:Ga Alpha-Detector," *IEEE SORMA West,* (Berkeley, CA) (June 2008).

D.11. D. Archer, C. Britton, Jr., N. Bull, M. Emery, M. Ericson, L. Fabris, E. Farquhar, S. Frank, D. Hurst, R. Lind, S. McConchie, J. Mihalczo, J. Mullens. E. Sword, and J. Radle, "The Imaging Detector Subsystem Electronics of the Fieldable Nuclear Materials Identification System (FNMIS)," *IEEE 2012 Nuclear Science Symposium* (Anaheim, California) (October 2012).

D.12. Paul Hausladen, Matthew Blackston, James Mullens, and John Mihalczo "Multimodal Imaging with Tagged Fast Neutrons for Material Identification" *Presentation 2012, CAARI 2012,* Aug 05, 2012–Aug 10, 2012, Ft. Worth, Texas (Aug 2012).

D.13. J. T. Mihalczo, E. D. Blakeman, G. E. Ragan, E. B. Johnson, and Y. Hachiya, "Dynamic Subcriticality Measurements Using the ^{252}Cf-Source-Driven Noise Analysis Method," *Nucl. Sci. Eng.*, **104**, no. 4, 314–338 (1990).
D.14. Z. Akcasu and A. Stolle, "Langevin Equation Approach to Reactor Noise Analysis: Stochastic Transport Equation," *Nucl. Sci. Eng.* **113**, no. 1, p 31–55 (1993).
D.15. J. P Weinman and M. R. Mendelson, "KAPL Monte Carlo Analysis of Subcritical Reactivity Measurements in the Oak Ridge Solution Tank," Knolls Atomic Power Laboratory, KAPL-M-7759 (September 1990).
D.16. E. D. Blakeman and T. E. Valentine, "Unreflected High Enriched Uranyl Nitrate Subcritical Noise Measurements" SUB_HEU_SOL_THERM-001, NEA/NSC/DOC/(95)03/II Volume II (2000).
D.17. E. D. Blakeman, "Subcritical Noise Measurements for Two Coaxial Cylindrical Tanks Containing 93.1 wt. % Uranyl Nitrate Solution," SUB_HEU_SOL_THERM-002, NEA/NSC/DOC/(95)03/II Volume II (2008).

APPENDIX E. BREAK FREQUENCY NOISE ANALYSIS AND PROMPT NEUTRON DECAY CONSTANT

This appendix has appeared on previous ORNL reports [E.1 and E.2] and is included here for convenience. This appendix defines the break frequency [E.3] and presents data from another measurement to show how the data is fitted [E.4] to determine the break frequency. The break frequency, sometimes called the cutoff frequency, is the frequency at which the response initiates its decrease[1]. This frequency is determined by fitting the cross or auto spectral densities to an amplitude and a break frequency. The data can be fitted to one break frequency because the point kinetics model is applicable, which is usually true for neutron multiplication factors above 0.80. At further subcritical, this model does not work because the data cannot be fitted in this manner to a single break frequency. This gives a quantitative estimate of when point kinetics interpretation cannot be used for this method.

The prompt neutron decay constants were obtained by simultaneously fitting the auto power spectral densities of detectors 2 and 3, the real and imaginary parts of the cross power spectral densities between the detectors and the source, and the real and imaginary parts of the cross power spectral densities between the two detectors. In this simultaneously fitting, all eight functions of frequency were corrected for the frequency response of the measurement systems. The frequency response was determined in separate measurements with only the source and two detectors spaced in air. This fitting determined the break frequency (fb), which is related to the prompt neutron decay constant (α) by the relation $\alpha = 2\pi fb$. The measured prompt neutron decay constants presented in Table B.1 increase in magnitude as the system becomes more subcritical. For some of the configurations, the prompt neutron decay constants were obtained from single mode fits of the measured spectra, while for other configurations two mode fits were performed for the measured spectra. Examination of the real and cross power spectral densities is plotted as the abscissa and the imaginary part is the ordinate, single mode decay, characterized by the resulting curve being in the fourth quadrant (i.e., real part > 0 and imaginary part < 0). Some results for one configuration of another experiment are given in Figures E.1 and E.2 [E.2]. A change of sign of either the real or the imaginary part of G12 signifies the presence of higher modes. The prompt neutron decay constants vary from 290 ± 9 inverse seconds at delayed critical to ~15,000 inverse seconds for a configuration of 289 fuel pins with 1,511 ppm boron. An example of some results of the fitting data from another experiment not related to this measurement is presented here to illustrate the fitting is given in Figures E.1 and E.2.

[1] https//en.wikipedia.org/wiki/cutoff_frequency.

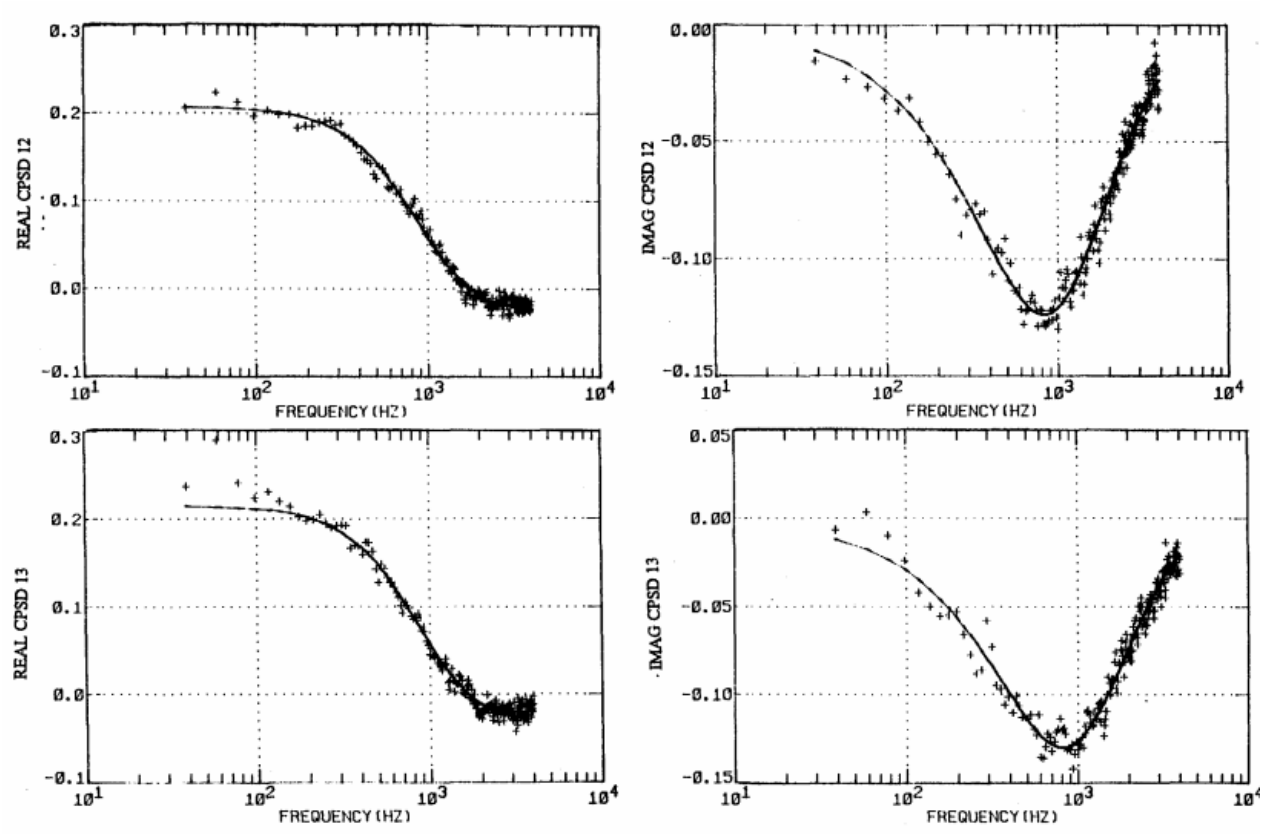

Figure E.1. Real and imaginary parts of the cross power spectral densities between the two detectors (2 and 3) and the californium source (1) for a fuel pin configuration of 4,962 fuel pins with a boron concentration of 2,386 ppm for detector 2 located at 30.4 cm SE–S–SW and detector 3 located at 30.4 cm NE–N–NW (the solid lines are the results of fitting all eight functions simultaneously).

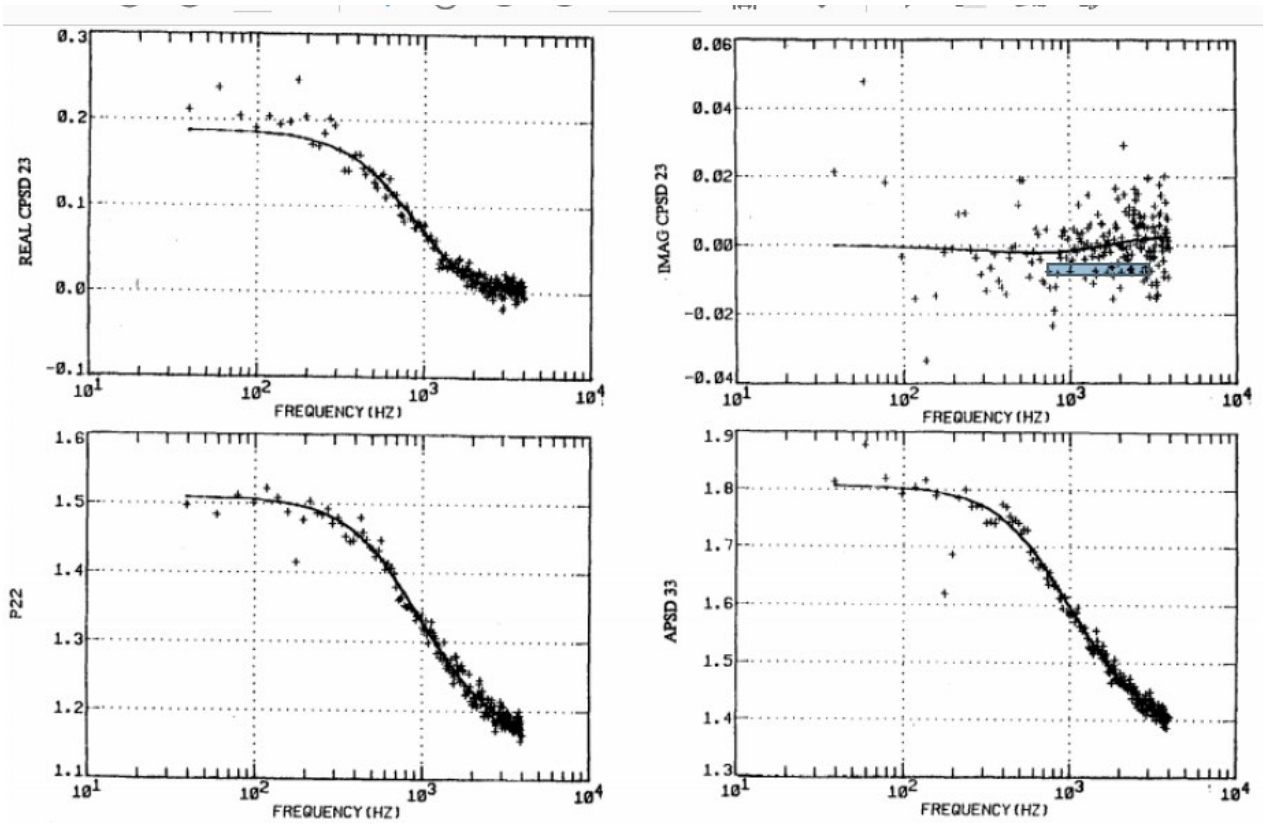

Figure E.2. Real and imaginary parts of the cross power spectral density between the two detectors (2 and 3). Auto power spectral densities for detectors 2 and 3 for a fuel pin configuration with a boron concentration of 2,386 ppm for detector 2 located at 30.4 cm SE–S–SW and detector 3 located at 30.4 cm NE–N–NW (the solid lines are the results of fitting all eight functions simultaneously).

REFERENCES

E.1. John T. Mihalczo, "Critical and Californium Source-Driven Noise Analysis Subcritical Measurements with an Unreflected Cylindrical Tank of Mixed Uranium-Plutonium Nitrate Solution" ORNL/TM-2021/1606 (June 2022).

E.2. John T. Mihalczo, "Subcritical Californium Source-Driven Noise Analysis Measurements with Unreflected Uranium (93.15) Hydride", ORNL/TM-2021/1963 (June 2021).

E.3. R. E. Uhrig, *Random Noise Techniques in Nuclear Reactor Systems*, The Ronald Press (January 1970).

E.4. John T. Mihalczo, "Critical and Subcritical Californium Source Driven Noise Analysis Measurements with PWR Fresh Fuel Pins", ORNL/TM-2021/1606 (Feb 2021).

APPENDIX F. PARAMETERS USED TO OBTAIN THE NEUTRON MULTIPLICATION FACTORS FROM THE RATIO OF SPECTRAL DENSITIES AT LOW FREQUENCY

The parameters used to obtain the neutron multiplication factor from the ratio of spectral densities at low frequency were obtained from KENO Monte Carlo calculations and are given in Table F.1. These data were calculations by E. D. Blakeman and from the author's notes.

Table F.1. Calculated parameters to infer neutron multiplication factors from the ratio of spectral densities at low frequency.

^{235}U (g/L)	I_c/I	Spatial effects correction (R)	Number of neutrons per induced fission	Lifetime[a] (10^{-4})	Effective delayed neutron fraction
13.70	2.3930	1.2737	2.40048	1.0701	0.0074302
12.89	2.3003	1.26527	2.40078	1.1825	0.0074326
12.37	2.3363	1.26839		1.1371	0.0074337
12.01	2.2751	1.26303		1.2210	0.0074378
11.07	2.2088	1.25526		1.3255	0.0074422
9.996	2.1342	1.24581	2.40083	1.4674	0.0074705
8.986	2.0614	1.23531		1.6348	0.0074503
7.935	1.9898	1.22384	2.40026	1.8494	0.0074548
6.505	1.8929	1.20622		2.2447	0.0074628
5.362	1.1125	1.18997		2.7352	0.00747001
4.448	1.7496	1.17595		3.3039	0.0074755
3.413	1.6798	1.15896		4.3073	0.0074794
2.531	1.6216	1.14320		5.8109	0.0074794
1.263	1.56	1.11993		11.642	0.0074841
0.632	1.4948	1.10860	2.40001	23.274	0.0074865
0.325	1.4762	1.10272	2.40002	45.221	0.0074885

[a]Neutron lifetime increases as the concentration is diluted more than the decrease with less fission. The neutrons take time bouncing around off hydrogen atoms before fission. This parameter is not needed for the interpretation but is given here since it was calculated as a function of solution concentration.